Evaluation of Electrical System Requirements for Implementing Turbine Electrified Energy Management

Jonathan L. Kratz [1], Dennis E. Culley[2], and George L. Thomas[3]
NASA Glenn Research Center, Cleveland, Ohio, 44135

Turbine Electrified Energy Management (TEEM) is a concept concerned with the management of energy in an electrified propulsion system. The management of energy in the hybrid-electric architecture has potential to benefit the turbomachinery and the aircraft it powers. The concept is particularly useful for improving operability during transient operation and could be leveraged to design a better performing engine. The concept utilizes electric machines coupled to the engine shafts and an electric power distribution system that includes energy storage. A controller is used to decide when and how energy is moved around the electrified propulsion system, particularly when considering energy conversion between mechanical and electrical forms. Prior work has shown that the electric machines can be used to supply/or extract supplemental power to/from the engine shafts to improve their operability and achieve or enable propulsion efficiency and performance benefits. However, the previous studies did not consider the practical constraints of the electrical machines and energy storage devices that are required for implementing the TEEM system architecture concept. This paper presents an integrated engine and electrical system model that is used to evaluate the electrical system requirements. The model captures the physics of the conceptual, Advanced Geared Turbofan 30,000lb$_f$ (AGTF30) engine, which features advanced technologies such as a compact gas turbine and a variable area fan nozzle. For this work, the engine is augmented with electrical system components that allow for the implementation of the TEEM concept. The evaluation presented suggests the potential of the TEEM concept to provide performance benefits for a turbofan engine.

Nomenclature

Alt	=	altitude, ft
C	=	bank capacitance, F
C_{SC}	=	capacitance of an individual super-capacitor cell or module, F
E	=	energy capacitor, kW-hr
E_U	=	useable energy capacity, kW-hr
E_{SC}	=	energy capacity of an individual super-capacitor cell or module, kW-hr
E_T	=	total energy capacity, kW-hr
$I_{Cont,SC}$	=	maximum continuous current of an individual super-capacitor cell or module, A
$I_{Peak,SC}$	=	maximum peak current of an individual super-capacitor cell or module, A
N	=	shaft speed, rpm
N_{HPS}	=	high pressure spool speed, rpm
N_{LPS}	=	low pressure spool speed, rpm
P	=	power, hp
SF_E	=	super-capacitor energy capacity safety factor

[1] Research Engineer, 21000 Brookpark Rd., Cleveland OH, MS-77-1, AIAA Member.
[2] Research Engineer, 21000 Brookpark Rd., Cleveland OH, MS-77-1, Senior AIAA Member.
[3] Research Engineer, 21000 Brookpark Rd., Cleveland OH, MS-301-5, AIAA Member.

SF_I = super-capacitor current safety factor
SF_V = super-capacitor voltage safety factor
SM = stall margin, %
SM_b = baseline stall margin, %
SM_{ben} = stall margin benefit expressed as a percentage of the stall margin improvement enabled by the electric machines, %
SM_u = stall margin with unconstrained electric machines, %
τ = torque, ft-lb_f
τ_{HPS} = torque applied by the electric machine on the high pressure spool, ft-lb_f
τ_{LPS} = torque applied by the electric machine on the low pressure spool, ft-lb_f
V_{FC} = voltage of the super-capacitor bank when it is considered to be fully charged, V
V_{Max} = absolute maximum bank voltage, V
$V_{Max,SC}$ = maximum voltage of an individual super-capacitor cell or module, V
V_{Min} = minimum bank voltage, V

I. Introduction

NASA is investigating the electrification of propulsion systems for commercial air transports, a sector that has previously been dominated by gas-driven turbomachinery. NASA has developed various hybrid-electric aircraft concepts that integrate turbomachinery with electrical hardware. These concepts often involve the use of electric machines (EMs), coupled to one or more of the engine shafts, to extract or supply power. Several of the concepts include energy storage, such as batteries, and consider a variety of electrical system architectures. Some concepts involve the use of electrically driven propulsors located in strategic positions on the aircraft to achieve aerodynamic benefits and higher propulsive efficiency. Ultimately, the conceptual studies have shown benefits with respect to reduced fuel burn, lower emissions, and/or reduced noise [1-5]. While the electrification of aircraft propulsion systems can produce benefits for the aircraft, it can also enable benefits for the turbomachinery that inevitably fold into aircraft level benefits such as reduced thrust specific fuel consumption. Turbine Electrified Energy Management (TEEM) is a concept that seeks to do just that by managing how energy is supplied to or extracted from the engine shafts based on the state of the engine and the demand from the pilot.. While TEEM was motivated by the emergence of hybrid electric propulsion concepts that already possess much of the electrical components necessary for implementation, the authors believe this technology to be applicable to more traditional gas turbine engines in the near term. This would demand that hardware necessary for implementing TEEM, economically justify its addition to the engine architecture if it is not already present. Such hardware may include electric machines (motors/generators), energy storage devices (ESDs) such as batteries and super-capacitors, and supporting electrical devices such as inverters, rectifiers, direct current–direct current (DC-DC) converters, cables, resistors, etc. It may also encourage dual use of existing components such as an electric starter motor, ESDs, and auxiliary power units (APUs).

At its broadest level, TEEM addresses the management of energy in an electrified turbine-based propulsion system. EMs coupled to the shaft(s) of the turbomachinery are used to selectively supply or extract torque in order to actively alter the operation of the engine. Thus, the TEEM concept can be viewed as an operability technology. Potential benefits of power addition/extraction during steady-state operation include, but are not limited to, the reduced need for stability bleeds and variable geometries, and expansion of the operating range of the engine. Power supplied/extracted during transients can alter the dynamic response. Done properly, transient stability margin can be reduced or even eliminated, thus enabling more efficient and better performing engine designs.

In prior work [6], the feasibility of the TEEM concept was demonstrated through application to the NASA-developed parallel hybrid-electric turbofan (hFan) [7,8] concept. While this was a modeling and simulation effort, it illustrated the anticipated impact of the technology. The documented study illustrated the elimination of the low pressure compressor stability bleed, or variable bleed valve (VBV), through energy management on the shafts. It also illustrated the application of EMs to selectively supply or extract power during engine transients in order to improve transient operability. A reduction or complete elimination of undershoot in compressor stall margin (SM) during engine transients was observed. Whereas open-loop torques were applied by the EMs in Ref. [6], Ref. [9] describes a closed-loop control approach for applying TEEM to a conceptual gas turbine engine model. The engine is known as the Advanced Geared Turbofan 30,000lb_f (AGTF30) [10], a two-spool geared turbofan engine representative of technology expected to enter service in the 2030-2035 time frame. The engine features a compact gas turbine and a variable area fan nozzle (VAFN). The dynamic engine model was executed in the MATLAB/Simulink® environment. It was developed using the Toolbox for Modeling and Analysis of Thermodynamics Systems (T-MATS)

[11] and was built to match the performance of the NASA N+3 reference engine [12] implemented in the Numerical Propulsion System Simulation (NPSS) code [13]. This paper expands on the work documented in Ref. [9].

The emphasis of Ref. [9] was the control approach for implementing aspects of the TEEM concept, but it made some assumptions about the electrical system, without consideration of hardware requirements, that may have resulted in an over-designed or under-designed system. Similarly it did not consider the limitations of the hardware that could result in unrealizable performance. This paper continues with the same application and control approaches discussed in Ref. [9], but it focuses on identifying basic requirements for the electrical system in order to assess the practicality of applying the TEEM concept on the chosen propulsion system. Requirements were developed through parametric studies that ultimately prompt a number of recommendations for the electrical components that either directly or indirectly imply several constraints. The study is focused on the requirements for the EM(s) that affect the shafts and the ESDs that supply or absorb the energy to do so.

Ref. [9] considers 3 configurations of the electrical system that were characterized by the number of EMs and variations in the shaft(s) they were coupled to. It considered EMs on both shafts or a single EM on either the low pressure spool (LPS) or the high pressure spool (HPS). These configurations are referred to as the dual-spool configuration, LPS configuration, and HPS configuration, respectively. Results from Ref. [9] showed that the LPS configuration could not practically affect the operability of the high pressure compressor (HPC) during acceleration transients. Furthermore, there were circumstances where the configuration required a large amount of power to be dissipated, thus requiring a large bleed resistor bank. For these reasons, the LPS configuration was not considered in this study. However, the dual-spool and HPS configurations were evaluated to assess if either configuration imposes different requirements. Two variants of the dual-spool configuration were considered. The first variant was consistent with the implementation in Ref. [9]. The second variant differed in the way it handled excess power dissipation during deceleration transients. The first variant sent the excess power extracted from the LPS to the ESDs until the ESDs were near full charge. Any additional power would be applied by the HPS EM. The second variant does not charge the ESDs during decelerations transients, but simply applies the excess power to the HPS spool via the HPS EM. It was hypothesized that this approach would reduce the power requirement of the LPS EM, thus reducing its size. To distinguish the two variations, they will be referred to as dual-spool configuration variant 1 (v1) and dual-spool configuration variant 2 (v2). In all configurations and variants, the EMs are assumed to spin at the same speed as the shaft they are coupled to.

A presentation of this paper begins with Section II. In Section II of this paper, a description of the models used in the study is presented. Included in the description is a discussion of the electrical system, its modeling, and its integration with the engine model. Section III provides a brief description of the TEEM control strategy. Section IV describes the studies conducted with the model and the results from those studies. Section V discusses tradeoffs regarding the TEEM system configurations and potential dual uses of TEEM hardware. Finally, Sections VI provides some concluding remarks.

II. System Modeling and Integration

In this study, two different models are utilized. Both apply the control strategy discussed in Ref. [9]. The controller used to apply this strategy will be referred to as the TEEM controller. The first model captures the physics of the AGTF30, but it lacks fidelity with respect to the electrical system. The model includes handles for affecting torque on the engine shafts, but does not model how the electrical system provides the required torque. It simply assumes that the electrical system supplies the torque that the engine needs. This model will be referred to as the engine-centric model. The second model is the engine-centric model integrated with electrical system component models. It will be referred to as the integrated model.

A. Engine-Centric Model

The AGTF30 engine represents a two-spool geared turbofan with a compact gas turbine and a VAFN. The engine model has been modified in a number of ways. Most notably it has been modified to accept inputs for supplemental torque on the engine shafts. First order dynamics, saturation limits, and rate limits were applied to the torque commanded by the TEEM controller to simulate EM dynamics. In all cases the EMs were assumed to have a bandwidth of 35 rad/sec. While much lower bandwidths were initially tested, the range of practical values did not have a significant impact on the ability of the TEEM controller to affect operability. The EM torque is supplied directly to the engine as an amount that is either added to or extracted from the shaft. The model does not consider how the EMs are supplied power, or how excess power extracted by the EMs is used or dissipated. The model simply assumes that the required power is supplied and that all excess power is absorbed or dissipated. The main parameters were the EM torque saturation limits and rate limits. The model was used to identify basic size and responsiveness requirements for

the EMs while also implying requirements for the rest of the electrical system. Since the responsiveness of the engine degrades over time, it is important to consider how this may impact the needs of the electrical system over the lifespan of the engine. Therefore, the engine-centric model incorporates a deterioration model that permits the adjustment of component health parameters in order to account for degradation. The deterioration model was adapted from the model applied to the Commercial Modular Aero-Propulsion System Simulation 40,000lb_f (C-MAPSS40k) engine model [14]. In the analysis to follow, a worst-case fully deteriorated engine was assumed. Degradation of electrical components was not considered in this study.

B. Integrated Engine and Electrical System Model

The critical components of the electrical system are the EMs and ESDs. However, there will also be various components to support the transfer of power between these devices. While these components were not the focal point of this study, they were modeled with the primary purpose of introducing realistic efficiencies/losses into the power transmission. These components can be grouped into a few categories. The first category is motor controller elements, which includes functions such as variable frequency inverters (DC-AC conversion) and rectification of alternating-current (AC-DC conversion). The second category is converters. This category may include devices such as direct current to direct current (DC-DC) converters and transformers. The third category is energy management elements and it may include devices such as bleed resistors and current/voltage limiting control circuits. The fourth and final category is power transmission elements which primarily consists of cables. A high level schematic of the electrical system is shown in Fig. 1, which assumes a DC power distribution system that includes a DC-DC converter. A particular electrical system architecture is assumed in this study, however it should be noted that the architecture and component parameters are merely a starting point for the systems design. Recall that the purpose of these studies is to evaluate feasibility through identification of electrical system requirements, not to perform a detailed system design. In a real world application, the implementation should be reconsidered to find the optimal system design. The architecture in this work consists of one EM for the HPS configuration and two EMs for the dual-spool configuration variants. The EMs can function as either a motor or generator. Energy storage is provided solely by a bank of super-capacitors. The power is transmitted through a DC bus whose voltage is regulated by a DC-DC converter. The EM control unit converts power from DC to AC to drive the EM(s) as motor(s) and from AC to DC when the EM(s) are acting as generator(s). Various cables connect the devices and transmit power through their conductors as needed.

The electrical system was modeled using the Electrical Modeling and Thermal Analysis Toolbox (EMTAT). EMTAT is currently under development at the NASA Glenn Research Center and has evolved from the electrical system modeling effort documented in Ref. [15] to perform power flow analysis on hybrid-electric systems. The toolbox is a Simulink library of electrical system components for capturing the interactions of turbomachinery and electrical systems at an appropriate level of fidelity. Such interactions include: (1) the coupling of EM torque/power dynamics with turbomachinery shaft dynamics, (2) charge and discharge cycles of ESDs, and (3) overall dynamic fluctuations of currents and voltages in the electrical system that occur in response to changes in electrical loads. The modeling time scale is often on the order of milliseconds, similar to the time scale used to model the turbomachinery

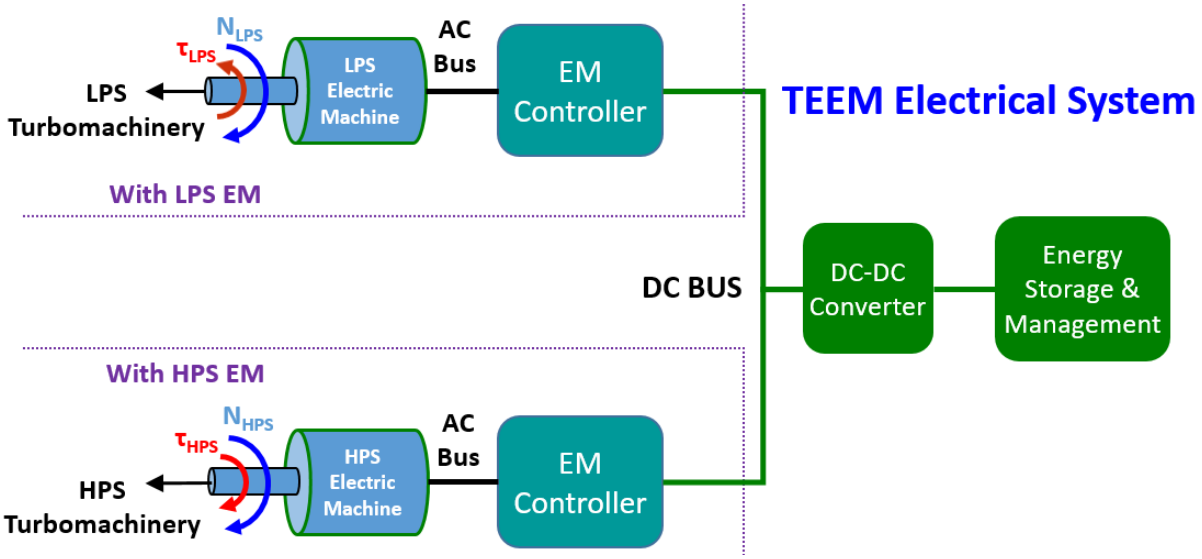

Fig. 1 TEEM electrical system with the HPS EM acting as a motor and the LPS EM acting as a generator [9]

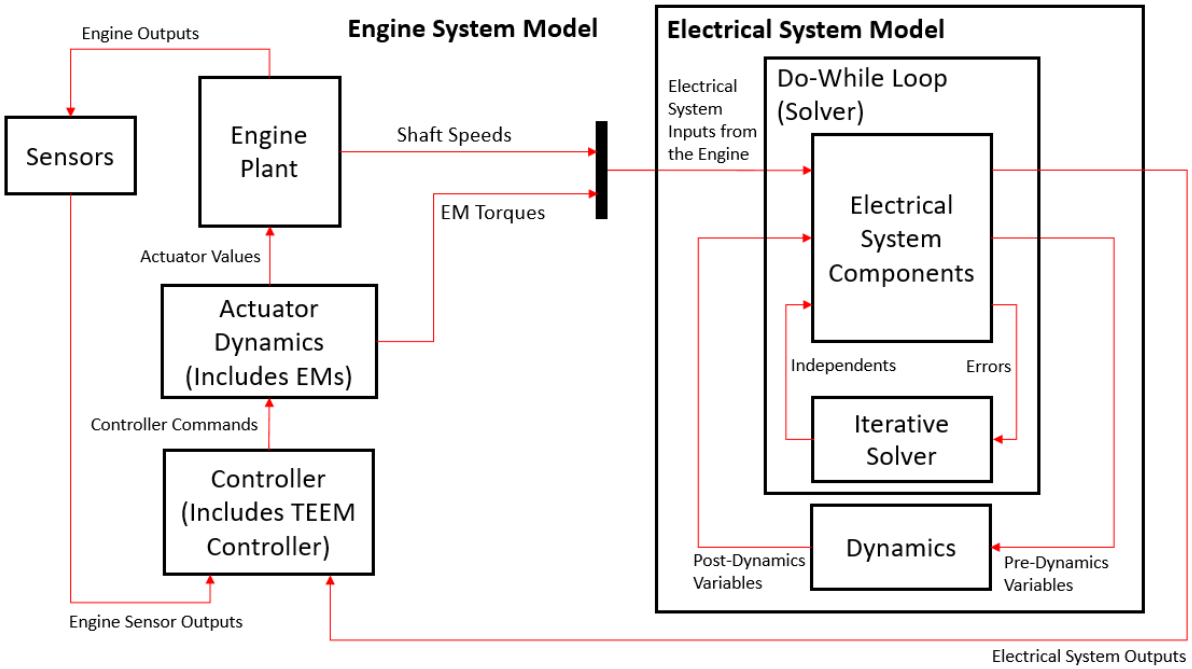

Fig. 2 Integrated engine and electrical system model

dynamics. Faster phenomena, such as those associated with switching circuits within the power system, are not modeled. However, bulk efficiencies are applied as an effort to approximate their overall impact.

The EMs are modeled with a constant impedance and a motor map that defines its efficiency at different speeds and torques. The inverter and rectifier models produce an output voltage that scales with frequency according to the specified flux constant. The load is assumed to have no inductance, thereby implying a unity power factor. The efficiency of the inverter/rectifier is specified by a look-up table that maps output current and voltage to efficiency. The DC-DC converter model is meant to produce a constant output voltage. Its efficiency is determined by a look-up table that is a function of input voltage and current. The input voltage is calculated such that power is conserved through the element. The super-capacitor bank is modeled with a specified capacitance, equivalent series resistance, and a constant leakage current. The rate of change in voltage of the capacitor is computed numerically inside the Simulink block given the voltage from the previous time-step. The various cables in the system are modeled with a simple impedance or resistance. Each block that represents an electrical component has an associated error and an independent

Table 1. Basic parameters of the electrical system model

Component	Parameter	Value
Super-Capacitor Bank	Capacitance	--
	Full Charge Voltage	--
	Equivalent Series Resistance	0.0031 Ω
	Leakage Current	0.04 A
DC-DC Converter	Bus Voltage	1000 V
	Maximum Efficiency	0.98
Bleed Resistor Bank	Resistance	0.5 Ω
Power Supply Cable	Resistance	0.001 Ω
Motor Cables	Resistance	0.001 Ω
LPS EM	Maximum Power	--
	Maximum Torque	--
	Maximum Torque Rate	--
	Maximum Speed	7500 rpm
	Maximum Efficiency	0.96
	Resistive Impedance	0.01 Ω
HPS EM	Maximum Power	--
	Maximum Torque	--
	Maximum Torque Rate	--
	Maximum Speed	23000 rpm
	Maximum Efficiency	0.96
	Resistive Impedance	0.01 Ω
LPS EM Inverter and Rectifier	Voltage/Flux Constant	0.996 V/Hz
	Maximum Efficiency	0.98
HPS EM Inverter and Rectifier	Voltage/Flux Constant	0.307 V/Hz
	Maximum Efficiency	0.98

variable that is typically a current or voltage associated with that component. A Newton-Raphson solver is used to adjust the independent variables to satisfy error tolerances. Dynamic variables, such as the super-capacitor voltage, are pulled out of the iterative solver subsystem to enforce the dynamics.

The overall structure of the electrical system model and its coupling to the engine model are presented in Fig. 2. The electrical system model consists of 3 levels: (1) the electrical component models, (2) the solver, and (3) the dynamics layer. The electrical system model receives the shaft speeds and electrical machine torques from the engine model. Prior to entering the electrical system model, first order dynamics, saturation limits, and rate limits are applied to the commanded torques. Thus the torques input to the electrical system model are the torques that are applied to the shafts. Some of the outputs of the electrical system are utilized by the TEEM controller, including the voltage across the super-capacitor bank or its state of charge.

The efficiency of the electrical machines was defined by maps relating the efficiency to the torque and speed. Similarly, the efficiency of the DC-DC converter and the inverters/rectifiers were defined by maps relating the efficiency to voltage and current. The maps were produced from an empirical characterization of a model of the Subsonic Ultra Green Aircraft Research (SUGAR) Volt hFan power system as presented in Ref. [16]. The basic parameters of the electrical system model are given in Table 1. The parameters that do not have an assigned numeric value were altered during the parametric study. Parameters having a numeric value remained fixed throughout the analysis.

III. TEEM Control Strategy

The TEEM control strategy in Ref. [9] has 2 primary functions: (1) improving transient operability, and (2) re-charging the ESDs. These goals must consider operability constraints, particularly at low power settings, thus requiring coordination with various actuator control schedules. Shown in Figure 3 is a high level schematic meant to capture the essence of the control approach. Note that "v1" in Fig. 3b refers to dual-spool configuration v1, while "v2" refers to dual-spool configuration v2. The white blocks signify high-level decision-making criteria while the blue blocks signify some action that is implemented if the appropriate criteria are met.

During transients, transient operability is prioritized while charging functions are temporarily suspended, and the low power stability issue is handled solely by the VBV, as it is in the baseline AGTF30 model. Active control of the EM(s) is applied via a gain-scheduled proportional integral (PI) controller that seeks to match the steady-state shaft speed vs. fuel flow or the low pressure compressor (LPC) pressure ratio (PR) vs. fuel flow relationship. LPC PR control is only applied during deceleration transients when there is a single EM on the HPS. The proportional and integral gains are scheduled based on Mach number (MN), altitude (Alt), and power lever angle (PLA). PLA is commanded by the pilot of the aircraft and corresponds to the engine's throttle position or power setting. In either configuration, power is input to the HPS during accelerations. For the dual-spool configuration, for which an EM is present on the LPS, power is extracted from the LPS during decelerations. Dual-spool configuration v1 directs the

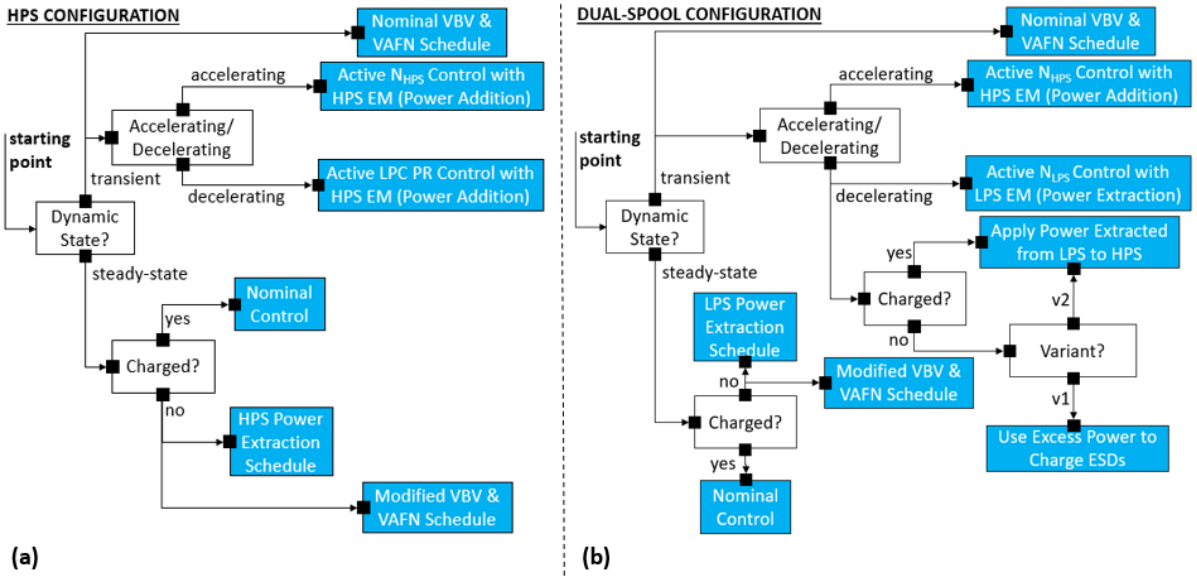

Fig. 3 High level schematic summarizing the TEEM control approach where (a) captures the HPS configuration and (b) captures the dual-spool configuration

extracted power to the ESDs until they are nearly charged and then begins expending the excess power by applying it to the HPS via the HPS EM. Dual-spool configuration v2 does not charge the ESDs, but instead applies all of the extracted power to the HPS via the HPS EM. The HPS configuration deals with both acceleration and deceleration transients by applying power to the HPS via the HPS EM.

During steady-state operation, the VBV solely handles the low power stability issue while the ESDs are sufficiently charged. When the devices are not sufficiently charged, an EM is used to extract power from one of the shafts to charge them. The amount of power extraction is set by a schedule. The power extraction is the same for most conditions but tapers to zero as the ESDs approach full charge. It is also reduced for very high engine power and very high altitude in order to preserve maximum thrust and ensure operability at high altitude. If an EM is present on the LPS then use of that device is the preferred means of power extraction. In either case, the VBV and VAFN schedules have been modified in order to maintain the same level of LPC and fan operability as the baseline AGTF30 while power is extracted from each shaft. For more details or clarification of the TEEM control strategy, refer to Ref. [9]. All parametric variants simulated in this study utilize the control logic presented here.

IV. Parametric Studies

A. Evaluation of EM Requirements

The EM requirements were considered first. The goal was to identify the maximum power, torque, and torque rate required for all applicable EMs, for each configuration considered. For conservative approximations, an end-of-life engine was assumed in the analysis. The first step was to identify the stall margin provided by the baseline engine and TEEM implementation via unconstrained EMs. In other words, the minimum stall margin achieved during transients with the baseline engine and with application of the TEEM concept using EMs that can instantaneously supply or extract whatever power is commanded. The difference between these values provides an indication of how much benefit the TEEM concept could potentially provide regarding the transient operability of the engine. When the EM is constrained, its benefit is expressed as a percent benefit as defined by Eq. (1).

$$SM_{ben} = \frac{SM - SM_b}{SM_u - SM_b} \times 100\% \tag{1}$$

In Eq. (1), SM is the minimum stall margin when the EM is constrained, SM_u is the minimum stall margin when the EM is unconstrained, and SM_b is the minimum stall margin of the baseline engine. This definition allows the results at various operating points to be normalized. In addition it provides a clear measure of how close the constrained results are to achieving the full benefit, thereby permitting identification of the EM requirements.

To determine the EM requirements, two sets of simulations were conducted, both with the engine-centric model. First, simulations were conducted for 20 select design points throughout the flight envelope to produce data that could be used to infer the EM requirements. Those points are identified in Fig. 4 by red plus signs. Second, simulations were conducted for 1000 test points throughout the flight envelope to verify that the TEEM controller was able to achieve the expected operability improvements with the selected EM constraints. Those test points are identified in Fig. 4 by blue x's. For each design point or test point, simulations were run for an idle to full throttle burst (acceleration) and a full throttle to idle

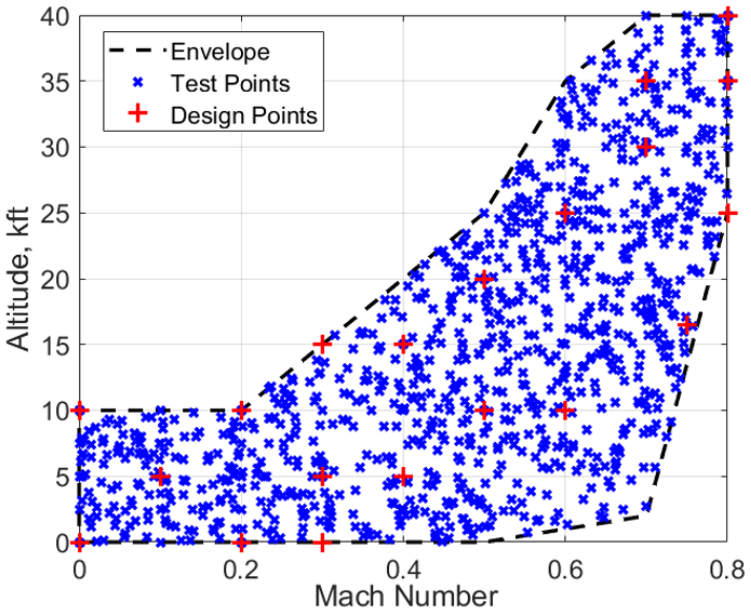

Fig. 4 AGTF30 flight envelope with design points used to size the EMs and test points used to verify sufficient EM performance throughout the flight envelope

chop (deceleration). In either case, the throttle position was ramped from its initial value to its final value over the course of 1 s. The first set of design point simulations varied the constraint on the maximum torque of the EMs. At the same time, constraints were placed on the maximum power setting that the EMs could apply and extract. The maximum HPS EM power constraint, in horsepower (hp), was set to be 3.75 times the maximum torque constraint in ft-lb_f. Similarly the maximum LPS EM power constraint, in hp, was set to be 1.25 times the maximum torque constraint in ft-lb_f. The scaling values of 3.75 and 1.25 were selected because they are approximately equal to the expected speeds of the respective shafts divided by the unit conversion factor of 5252 in Eq. (2), where P is the power in hp and N is the speed of the shaft in rpm. Thus, they are approximate scaling factors that relate the EMs power and torque.

$$P = \tau \frac{N}{5252} \tag{2}$$

A root finding technique, known as the bisection root method, was used to numerically adjust and identify the minimum torque required to achieve 98%, 95%, and 20% of the stall margin benefit. For accelerations, the HPC SM was used for the SM_{ben} calculation and the HPS EM torque limit was adjusted by the root finding method. During decelerations, the LPS SM was used for the SM_{ben} calculation and the HPS EM or LPS EM torque limit was adjusted by the root finding method, dependent upon the configuration. Once the torques were identified, simulations were conducted for a number of torque constraints between the 20% and 95% solutions in order to complete the data set. This data was used to produce the plots shown in Fig. 5, which were used to subjectively choose the minimum torque requirement for each EM. The recommendations for achieving nearly all of the benefit are provided in Table 2.

The maximum torques for the EMs were fixed at the values identified previously Simulations were run at the same design points in the same manner as before, but this time the maximum torque rate constraints were varied instead of the maximum torque constraints. Once again, the bisection root method was used to numerically identify the minimum

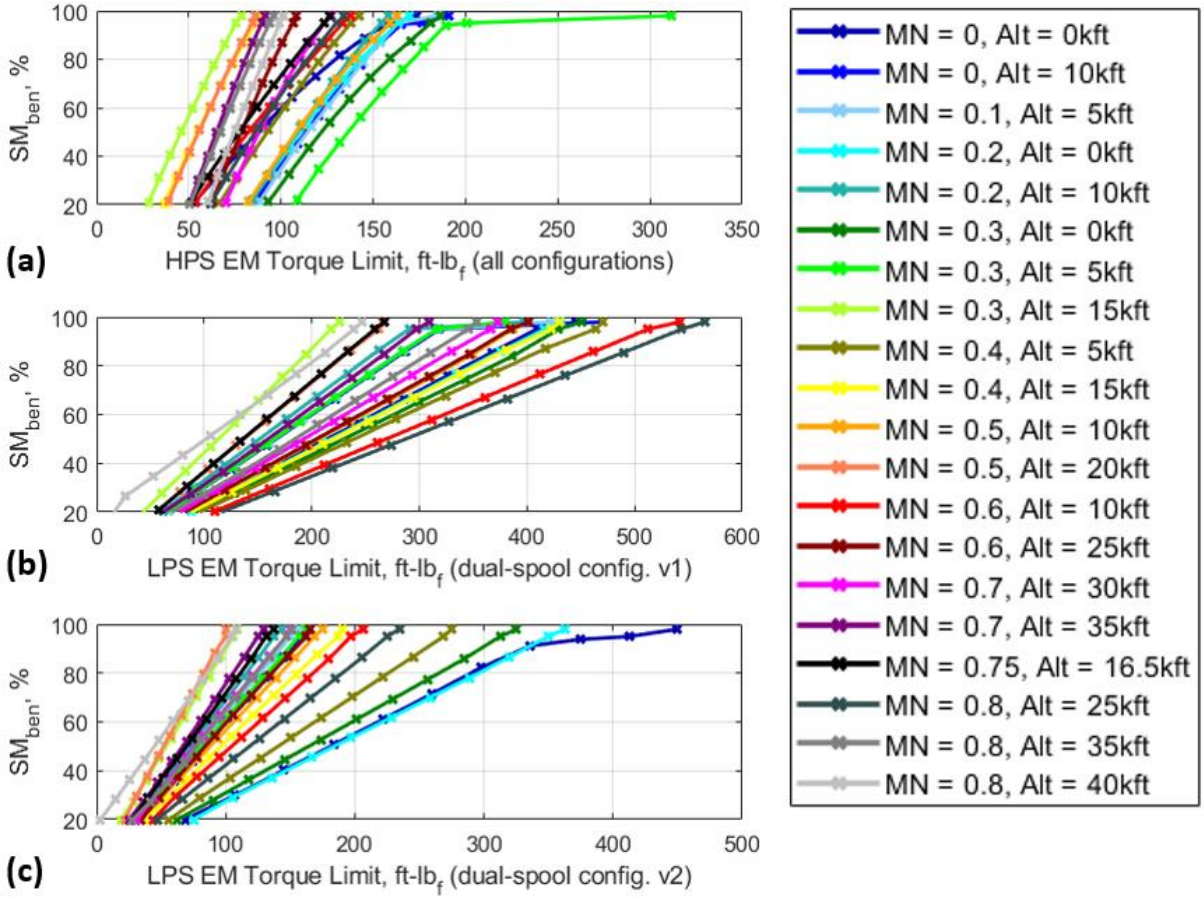

Fig. 5 Stall margin benefit versus EM torque limits for the HPS configuration (a), dual-spool configuration v1 (b), and dual-spool configuration v2 (c)

Table 2. Electric machine requirements

Electric Machine	Maximum Torque, ft-lb_f	Maximum Power , hp	Maximum Torque Rate, ft-lb_f/s	Time to achieve Maximum Torque, s
HPS EM	200	750	250	0.8
LPS EM (dual-spool v1)	550	610	150	3.7
LPS EM (dual-spool v2)	350	410	95	3.7

torque rate required to achieve 98%, 95% and 20% of the stall margin benefit at each of the test points for both the acceleration and deceleration transients. Simulations were run with different torque rate constraints between the 20% and 95% solutions in order to complete the data set. The results from these simulations are shown in Fig.6. From these plots, the recommendations for maximum torque rate were inferred and recorded in Table 2. The maximum torque and torque rate allow for the minimum response time of the EM to be inferred. These values are recorded in Table 2 and they represent the approximate minimum times to achieve the maximum torque output when starting from zero torque. EMs are known to have a very quick torque response time. Response times on the order of seconds, as required here, are not expected to be an issue.

To verify that the constraints identified for the test cases are valid, the constraints were applied for the 1000 random flight envelope points indicated in Fig. 4. Figure 7 presents plots of the HPC SM and LPC SM improvement over the baseline engine for these simulations. As can be seen, substantial SM benefits are achieved throughout the flight envelope. With the enforced constraints, implementation of the TEEM concept would allow for 2.5% to 5.75% HPC SM and up to 3.75% LPC SM to be removed from the transient operability stack. Note that at high Mach number and low altitude, the LPC SM improvement approaches zero because the LPC SM undershoot for the baseline engine

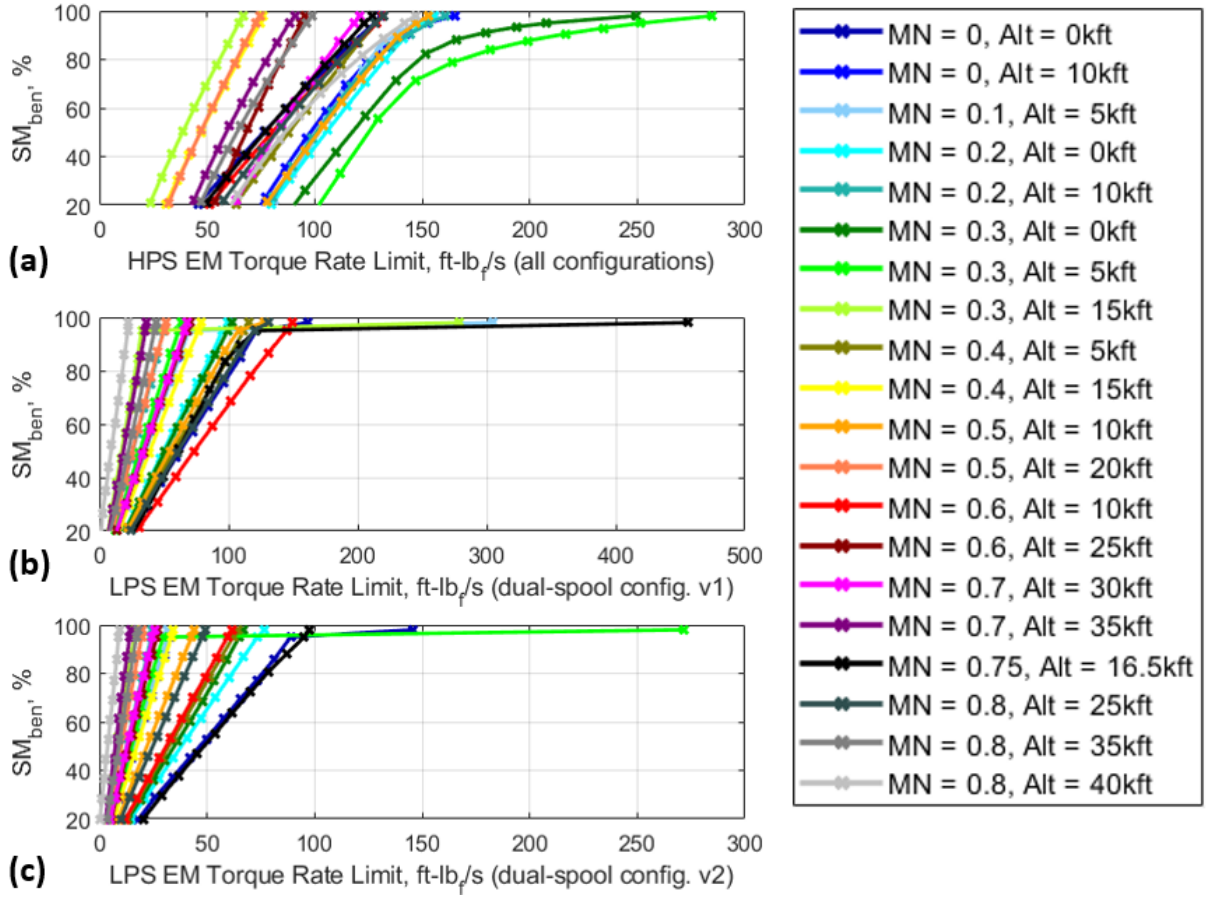

Fig. 6 Stall margin benefit versus EM torque rate limits for the HPS configuration (a), dual-spool configuration v1 (b), and dual-spool configuration v2 (c)

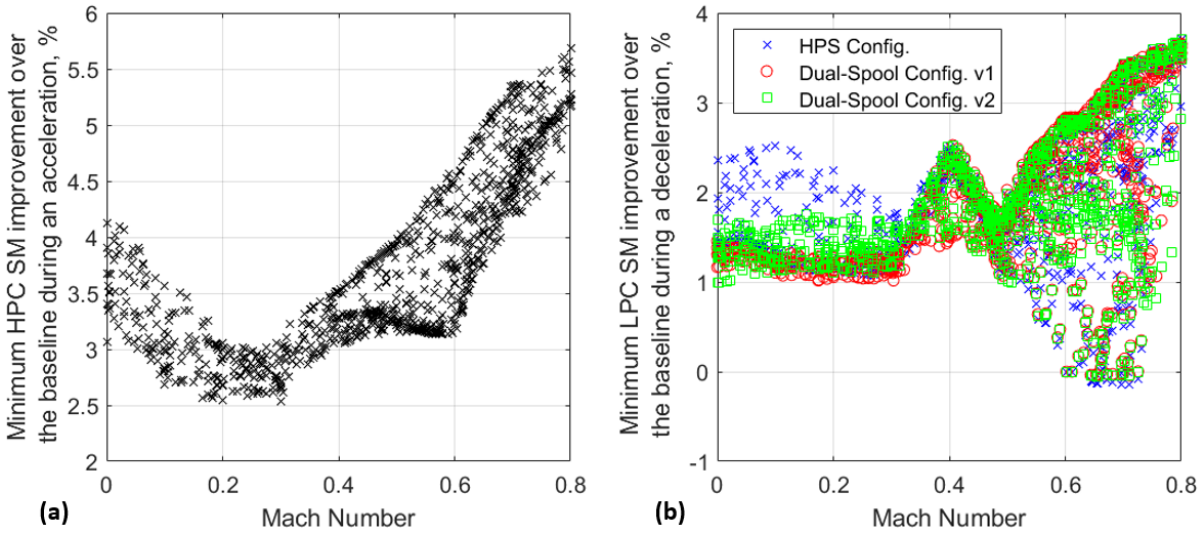

Fig. 7 HPC SM (a) and LPC SM (b) improvements over the baseline engine with constrained EMs

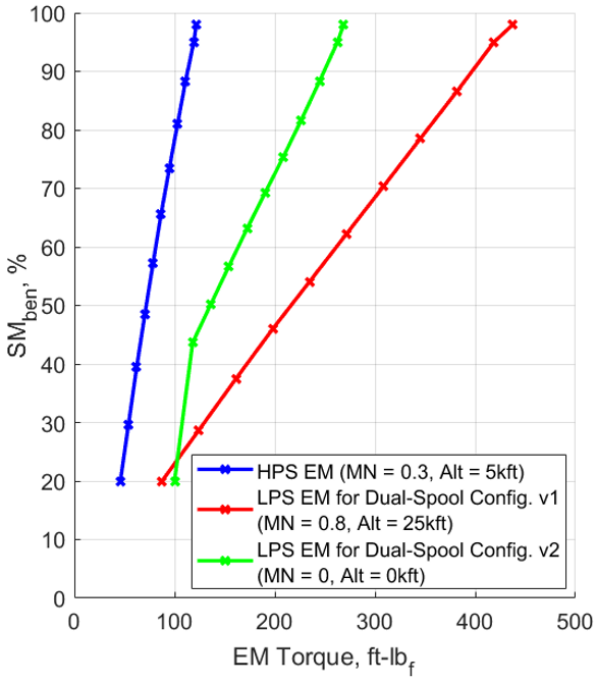

Fig. 8 Stall margin benefit versus EM torque limits for a new engine at the worst observed design points

approaches zero. Therefore, the potential for improvements approach zero. Furthermore, the steady-state stall margin at these flight conditions includes additional margin in comparison to other flight conditions. While the minimum LPC SM is reduced by < 0.1% in some instances with the HPS configuration and dual-spool configuration v2, this small decrease to operability is not of concern. In addition, these operational considerations are not typical of a commercial transport mission and therefore would be unlikely to be encountered. The simulation data was analyzed to see if the maximum power constraint was reached. If not, the power constraint enforced previously could be relaxed. While the HPS EM power constraint was reached in the simulations, the LPS EM power constraint was not. This prompted a relaxation in the maximum power requirement for both of the dual-spool variants. The final recommendations on the maximum power requirement are recorded in Table 2.

Recall that the recommendations for EM requirements were made assuming a worst-case end of life engine. It is worth noting that the requirements would have been substantially lower had the analysis been conducted for a new engine. To illustrate this point, Fig. 8 shows the stall margin benefit versus torque limit for a new engine at the design point at which the most torque was required for the end of life engine. The torque and power limits were reduced to 120 ft-lb_f (~450 hp) for the HPS EM in all configurations. The LPS EM torque and power limit was reduced to 420 ft-lb_f (~465 hp) for dual-spool configuration v1, and 250 ft-lb_f (~290 hp) for dual-spool configuration v2. This equates to a reduction in power requirements of 30 – 40%.

B. Evaluation of Super-Capacitor Requirements

Once the EM requirements were determined, focus was directed toward determining the super-capacitor requirements. The super-capacitors need to collectively supply or absorb power as the EMs demand. This means that they need to be capable of storing a sufficient amount of energy to address engine transients while also handling large peak currents. The super-capacitor bank was assumed to be structured into n_p strings of super-capacitors that are in

parallel with each other. Each string has n_s super-capacitors in series. It is possible that each super-capacitor in the bank could consist of multiple cells arranged in a similar fashion. Some consideration was given to redundancy for fault handling. If a string should fail, the remaining strings should be able to handle the current demand and there should be enough energy capacity to handle a worst-case transient. Also, if a cell within a string were to short circuit, the other cells within that string should be able to safely increase in voltage such that the desired bank voltage can be achieved. To address these potential situations, current, energy, and voltage safety factors (SF_I, SF_E, and SF_V) were applied as defined by Eq. (3) and (4).

$$SF_I = SF_E = 1 + \frac{1}{n_p - 1} \tag{3}$$

$$SF_V = 1 + \frac{1}{n_s - 1} \tag{4}$$

For this study, the peak current of the individual super-capacitors, $I_{Peak,SC}$, was assumed to be 1900 A based on the capabilities of super-capacitors modules that are currently available [17]. The minimum amount of useable energy that the super-capacitors should have is a bit subjective. For this analysis it was assumed that the super-capacitors should have enough useable energy capacity to handle a worst-case transient for an end-of-life engine. It is a bit subjective as to how to define the worst-case transient. Considering the 1000 test cases run during the analysis of the EM requirements, the maximum energy required for an acceleration transient was ~1.3 kW-hr. The worst-case point occurs at high altitude and high Mach number, a scenario in which an extreme acceleration transient is unlikely. Thus, there could be an argument to narrow the search for a worst-case scenario down to more likely scenarios, such as take-off or an aborted landing. Narrowing the search range for a worst-case scenario to Mach numbers below 0.3 and altitudes below 15,000 ft, the amount of useful energy capacity could be reduced to ~0.8 kW-hr. During the decelerations, the HPS configuration applies power, which could arguably drive up its energy capacity requirements. Considering the entire flight profile, ~2 kW-hr of energy is applied during the worst-case deceleration transient. For the reduced search range, the energy drops to 1.6 kW-hr. To address a scenario in which the pilot could rapidly reduce the power immediately following an acceleration transient, the total amount of useful energy capacity should be greater than 3, and 2.5 kW-hr when considering the entire flight envelop and the reduced search range, respectively. Once again, this would be an unlikely scenario. Therefore, an argument could be made to completely disregard the combination of transients and only focus on the transient scenario(s) for which there is a reasonably significant chance of occurring. The results are summarized in Table 3. Based on observation of the LPC SM response, it is suspected that the HPS EM controller, used for deceleration transients in the HPS configuration, commanded more power than is necessary to achieve the operability goals. Thus, it was noted that further attention to the design of this controller would reduce the energy usage during decelerations.

Table 3. Super-capacitor recommended useful energy capacities

Worst-case energy used during transients, kW-hr			
Worst-case search range	Acceleration	Deceleration (HPS configuration only)	Total (HPS configuration only)
Entire Flight Envelope	1.3	2	3
MN < 0.3, Alt < 10,000 ft	0.8	1.6	2.5

The following analysis of the super-capacitor parameters focuses primarily on a useful energy capacity E_U of 0.8 kW-hr. However, the parametric analysis can be easily performed for other values of useful energy capacity following the same analysis procedure. The energy requirements are believed to be conservative, noting that energy usage is expected to be much less during typical operation of the engine. To put this into perspective, Ref. [9] applied the TEEM concept to a mid-life engine and simulated a flight with a duration of nearly 1 hr and 40 min. During that flight, only 0.34 to 1.7 kW-hr was used in total. The largest expenditure of energy during a single transient was ~0.2 kW-hr with a maximum applied power of less than 200 hp.

In the parametric analysis, n_s, n_p, the bank equivalent capacitance C, and the power extraction for charging P_c were varied to study their impact on the following: minimum bank voltage V_{Min}, full charge bank voltage V_{FC}, absolute maximum bank voltage V_{Max}, total bank energy capacity E_T, individual super-capacitor maximum voltage $V_{Max,SC}$, individual super-capacitor energy capacity E_{SC}, individual super-capacitor capacitance C_{SC}, and the individual super-capacitors maximum continuous current $I_{Cont,SC}$. The full charge bank voltage is defined in this analysis as the voltage at which the super-capacitor bank is considered to be at full charge. This value will be lower than the absolute

maximum bank voltage, which is higher to address potential fault scenarios. The calculation of each of the parameters listed prior will be discussed next along with a visualization of their parametric variation.

The individual super-capacitor capacitance was computed with Eq. (5).

$$C_{SC} = C\frac{n_s}{n_p} \qquad (5)$$

Figure 9 plots the relationship to visualize the individual super-capacitors capacitance in order to achieve the desired bank capacitance. More super-capacitors in series correlates to lower bank capacitance while more super-capacitor strings in parallel correlates to more bank capacitance. To keep the current demand from exceeding the limitation of the individual super-capacitors, a minimum bank voltage requirement needs to be imposed. This means that a portion of the energy within the super-capacitors should be kept in reserve. The minimum voltage was calculated using Eq. (6).

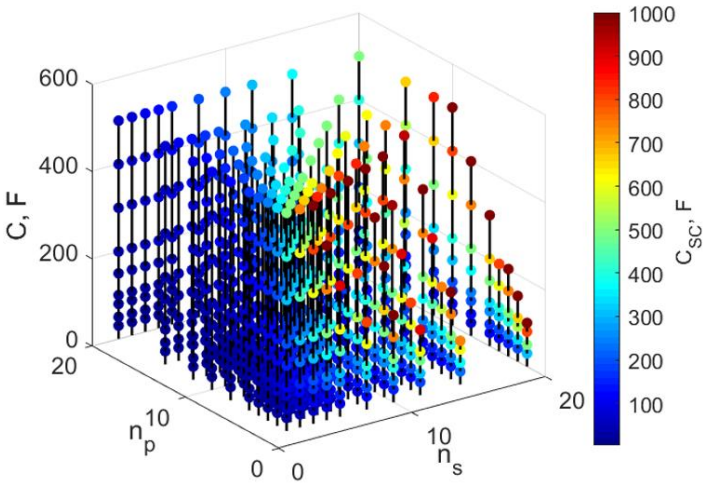

Fig. 9 Individual super-capacitor capacitance

$$V_{Min} = \frac{745.7P_{max}/0.9}{n_p I_{Peak,SC}/SF_I} \qquad (6)$$

Here P_{max} is the maximum power draw (750 hp) and the factor of 0.9 is introduced to account for power losses during power transmission. Figure 10 shows the minimum bank voltage plotted as a function of n_p. As n_p increases, V_{Min} decreases. This is due to the current safety factor, which reduces as the number of strings increases because there are more strings to share the current load if a single string were to fail.

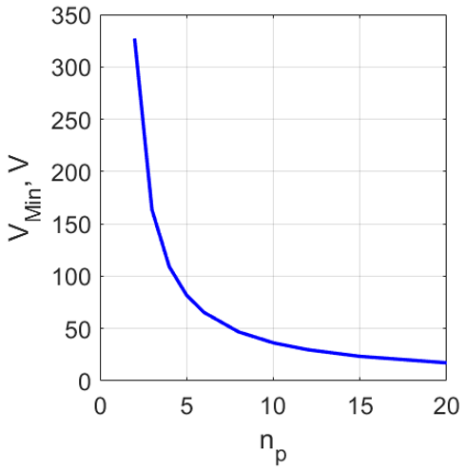

Fig. 10 Minimum bank voltage

A conservative limit on the maximum continuous individual super-capacitor current is given by Eq. (7).

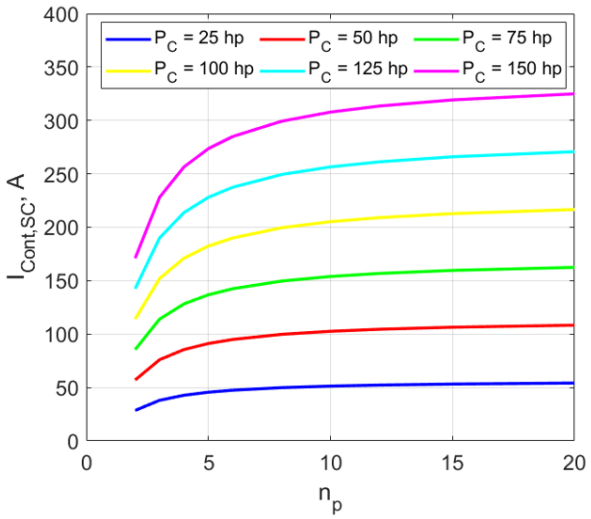

Fig. 11 Maximum continuous super-capacitor current

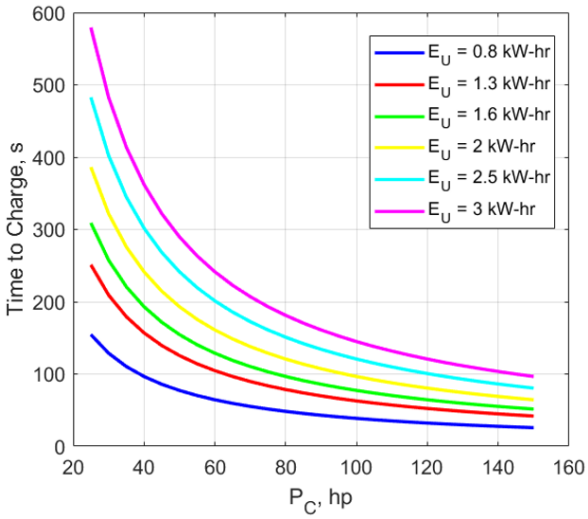

Fig. 12 Time to charge

$$I_{Cont,SC} = \frac{745.7 P_C}{n_p V_{Min}} \quad (7)$$

Since transients are short, power addition or extraction during transients should not drive the $I_{Cont,SC}$ requirement. In the current control strategy, charging the super-capacitors is the only mode of operation that has the potential to require current flow to or from the super-capacitors for an extended period of time. Thus the charging power is used to compute the maximum continuous current. The estimate is conservative because V_{Min} will increase as super-capacitors charge, thus the limit would only be reached for an instant. Figure 11 plots the variation of $I_{Cont,SC}$ with n_p and P_C. To provide some context for the difference between the different charging rates, Fig. 12 shows the approximate time required to reach the full charge bank voltage from the minimum bank voltage. This figure also gives an indication of how closely in time extreme transients can occur. Ideally, subsequent extreme transients will be spaced apart such that the super-capacitor has time to re-charge.

The full charge bank voltage must be sufficient to achieve the desired amount of useful energy capacity. The maximum bank voltage must also account for the voltage safety factor defined in Eq. (4). The total energy capacity of the super-capacitor bank must allow the maximum absolute bank voltage to be achieved. Equations (8), (9), and (10) were used to calculate the values of each of the respective parameters.

$$V_{FC} = \sqrt{\frac{2}{C}\left((3.6 \times 10^6) E_U SF_E + \frac{1}{2} C {V_{Min}}^2\right)} \quad (8)$$

$$V_{Max} = SF_V V_{FC} \quad (9)$$

$$E_T = \frac{1}{2} C {V_{Max}}^2 \quad (10)$$

Figure 13, 14, and 15 show the variation of each of these parameters with respect to C, n_s, and n_p, assuming E_U to be 0.8 kW-hr. While specific recommendations are not given, some general conclusions suggest that the higher the number of super-capacitor cells or modules, the lower the overall maximum voltage and total energy capacity. Also, putting capacitor strings in parallel is more beneficial than putting the capacitors in series.

With a better understanding of the bank requirements, a few more individual super-capacitor parameters can be evaluated; specifically, $V_{Max,SC}$ and E_{SC} which were computed using Eq. (11) and (12).

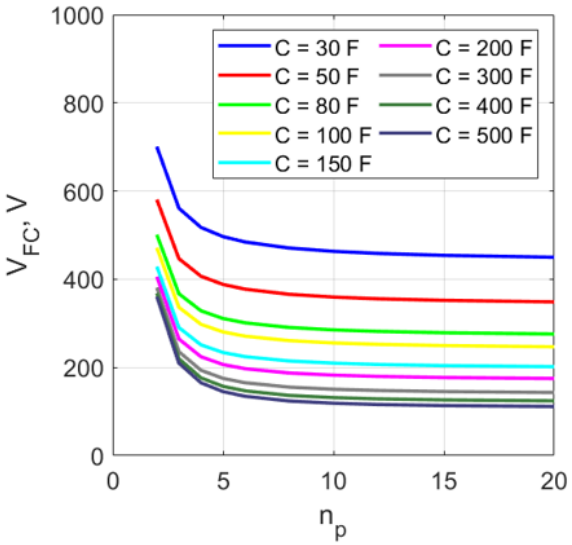

Fig. 13 Full charge bank voltage

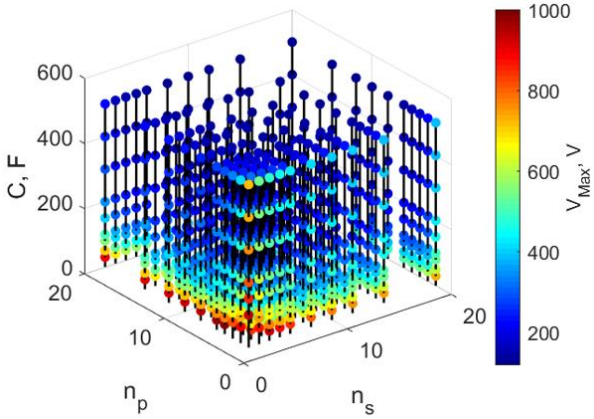

Fig. 14 Maximum bank voltage

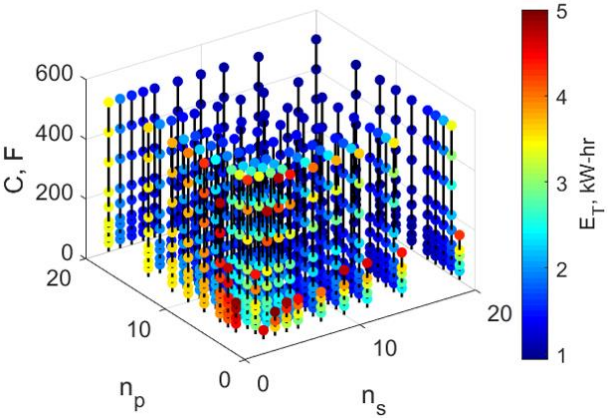

Fig. 15 Total bank energy capacity

$$V_{Max,SC} = V_{Max}/n_s \quad (11)$$

$$E_{SC} = (2.78 \times 10^{-7}) \times \frac{1}{2} C_{SC} {V_{Max,SC}}^2 \quad (12)$$

Figure 16, and 17 show the variation of each of these parameters with respect to C, n_s, and n_p assuming E_U to be 0.8 kW-hr. The maximum voltage of the individual super-capacitors is strongly impacted by n_s, which decreases as n_s increases.

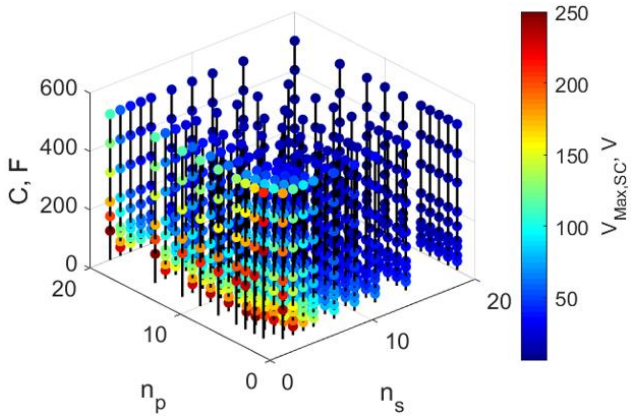

Fig. 16 Super-capacitor maximum voltage

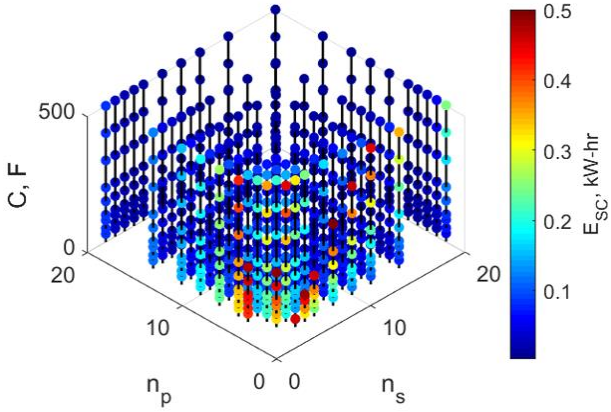

Fig. 17 Super-capacitor energy capacity

C. Integrated Model Test

Based on the results presented to this point, a set of electrical system parameter values were chosen for simulation with the integrated model. Those system parameters are listed in Table 4. The amount of useful energy capacity was

Table 4. Integrated model parameters selected for testing

Component	Parameter	Value		
		Dual-Spool Config. v1	Dual-Spool Config. v2	HPS Config.
Super-Capacitor Bank	Number of Super-Capacitors in Series	6		10
	Number of Super-Capacitor Strings in Parallel	12		15
	Useful Energy Capacity	0.8 kW-hr		2.5 kW-hr
	Bank Capacitance	100 F		75 F
	Minimum Bank Voltage	30 V		23 V
	Full Charge Bank Voltage	252 V		508 V
	Maximum Bank Voltage	303 V		564 V
	Total Bank Energy Capacity	1.27 kW-hr		3.31 kW-hr
	Super-Capacitor Capacitance	50 F		50 F
	Maximum Super-Capacitor Voltage	50 V		56 V
	Super-Capacitor Energy Capacity	0.018 kW-hr		0.022 kW-hr
	Maximum Super-Capacitor Continuous Current	174 A		177 A
	Charging Power	75 hp		
	Super-Capacitor Peak Current	1900 A		
LPS EM	Maximum Power	610 hp	410 hp	N/A
	Maximum Torque	550 ft-lb_f	350 ft-lb_f	N/A
	Maximum Torque Rate	150 ft-lb_f/s	90 ft-lb_f/s	N/A
HPS EM	Maximum Power	750 hp		
	Maximum Torque	200 ft-lb_f		
	Maximum Torque Rate	250 ft-lb_f/s		

set to 0.8 kW-hr for the dual-spool configuration variants and 2.5 kW-hr for the HPS configuration. Note that the selected parameter values are for demonstration purposes and are not meant to represent a realistic physical system. The test case was chosen to be at a Mach number of 0.2 and an altitude of 5,000 ft. These conditions are consistent

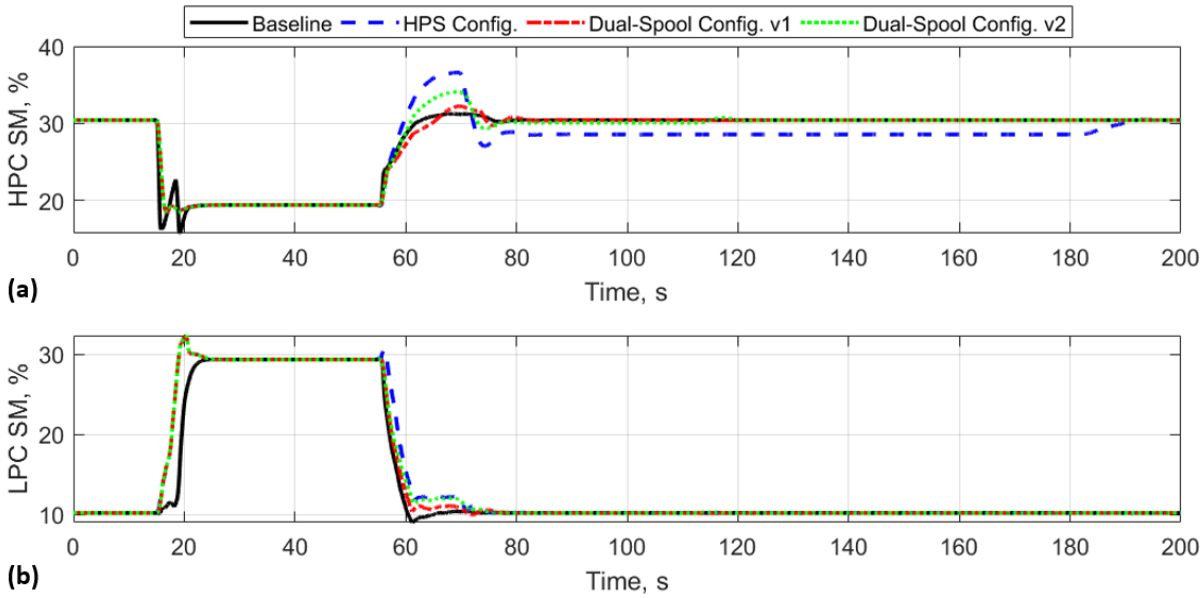

Fig. 18 HPC SM (a) and LPC SM (b) responses for a burst and chop at a Mach number of 0.2 and an altitude of 5,000 ft

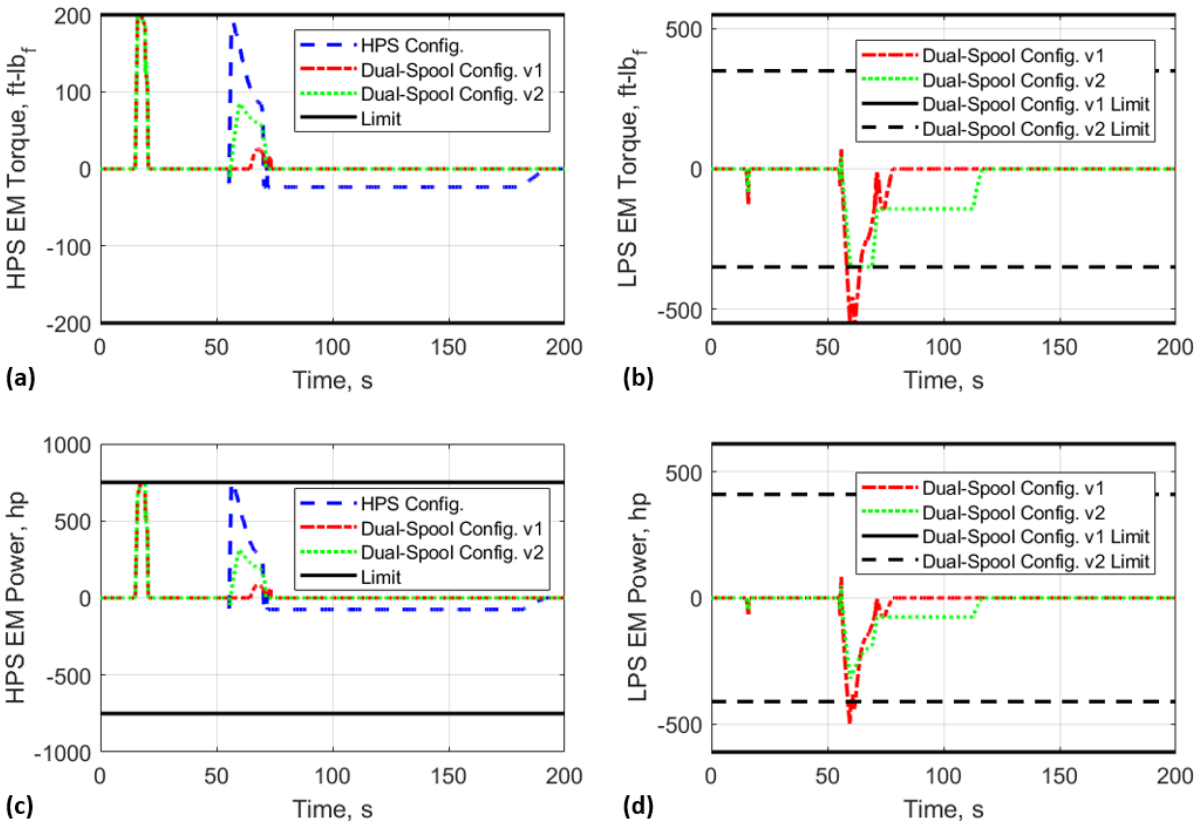

Fig. 19 EM torque and power responses for a burst and chop at a Mach number of 0.2 and an altitude of 5,000 ft. HPS EM torque and power are plotted in (a) and (c), respectively. LPS EM torque and power are plotted in (b) and (d), respectively.

with an aborted landing scenario at a high altitude airport, which could be a potential worst-case design scenario. The power level was increased from idle to full throttle over a duration of 1 s. After a brief time at the maximum power, the power was returned to idle over a period of 1 s. Figure 18 shows the stall margin variations compared to the baseline engine. Generally speaking, the minimum stall margins were increased. Note that the HPC SM is reduced during the charging period of the HPS configuration. Figure 19 shows the EM torque and power responses. The plots verify that the EM constraints were not exceeded. The power extraction observed after the deceleration was for charging the super-capacitors. Finally Fig. 20 shows the super-capacitor bank voltage and current to verify that the voltage and current limits were not exceeded. Note that the current plotted in Fig. 20 is the individual super-capacitor current, not the overall current going through the entire bank.

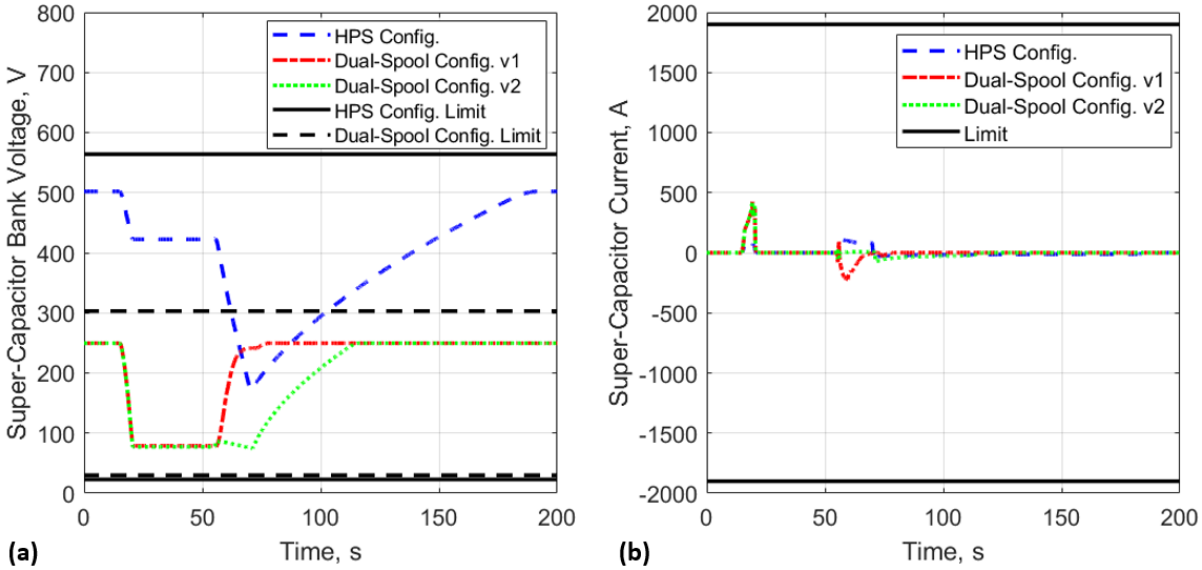

Fig. 20 Super-capacitor voltage (a) and current (b) responses for a burst and chop at a Mach number of 0.2 and an altitude of 5,000 ft

V. Discussion

In-direct and direct electrical system recommendations have been made for the implementation of the TEEM concept. Primary results include the suggestion for a 750 hp HPS EM with the ability to achieve maximum torque within 0.8 s. For dual-spool configuration v1, a 610 hp LPS EM is suggested with the ability to achieve the maximum torque within 3.7 s. The alternative variant, dual-spool configuration v2, allowed the LPS EM power to be reduced to 410 hp. Power need only be applied for the short duration of the transients, so it is possible that an undersized EM could be used as long as the EM's peak power capability is sufficient. Furthermore, the analysis considered a fully deteriorated engine. Simulation data showed that, with the deterioration applied in the model, the EM requirements for a new engine were 30-40% lower than what is prescribed here. Based on this observation, trades could be made between component sizing and engine maintenance practices. Alternatively, it might be worth considering the use of different sized/powered EMs on the engines as it ages, or perhaps installing additional EMs on the spool(s) in order to provide the additional required torque as the engine ages. It is also worthwhile to consider the variability of the system requirements in response to the deterioration model, and whether those variations are realistic.

While it is unclear how conservative the super-capacitor requirements will need to be, suggestions can be made based on the recommended power levels of the EMs and the energy required during a worst-case transient scenario. Parametric analysis has provided data on the super-capacitor bank and individual cell or module parameters as well as the power extraction used for charging the super-capacitors. Conclusions drawn from the results are somewhat subjective and therefore specific suggestions are not provided. However, the results could be used to study trades in super-capacitor parameters that could drive development or selection in a given application. The analysis assumed that the individual super-capacitors were capable of handling a peak current of 1900 A based on the capabilities of present day super-capacitors. If the peak current capability were more, its impact would generally be a reduction in the super-capacitor requirements. Because the ESD requirements are heavily driven by the EM requirement, the same arguments regarding deterioration that applied to the EMs, also apply to the super-capacitors. In other words,

significantly less energy storage would be required for a new engine than for an end-of-life engine, which implies potential trades between component sizing and maintenance practices. Once again, it is also worthwhile to consider if the deterioration model in this application is producing unrealistic variability in the engine performance that is producing overly conservative requirements.

There is an interesting tradeoff between the configurations. Dual-spool configuration v2 reduces the power requirement of the LPS EM by ~33% compared to dual-spool configuration v1. However, dual-spool configuration v1 allows for power extracted during transients to be used to charge the ESDs, making more efficient use of the extracted power. While the HPS configuration eliminates the need for an LPS EM, it may require the super-capacitors to have significantly more energy storage because power is applied during both the acceleration and deceleration transients. Thus there is a tradeoff between the HPS and dual-spool configurations. To help quantify the tradeoff, 0.8 to 1.3 kW-hr of usable energy is suggested for the dual-spool configurations and 1.6 to 3 kW-hr of usable energy is suggested for the HPS configuration, depending on how the worst-case transient scenario is defined. At minimum, the HPS configuration would trade a 410 or 610 hp EM for 0.8 to 1.7 kW-hr of super-capacitors. The energy storage would actually need to be larger than this considering the need to over-design for potential failure modes and to maintain a minimum bank voltage in order to prevent the current from exceeding its limits. Considering that the power density of EMs is expected to be about 9 kW/kg (5.5 hp/lb_m) [18] and the energy density of super-capacitors is ~0.1 kW-hr/kg (0.0045 kW-hr/lb_m) and more typically ~0.05 kW-hr/kg (0.00225 kW-hr/lb_m), the tradeoff appears to be in favor of the dual-spool configuration. However, there is potential to drastically improve the energy density of super-capacitors. Ref. [19] summarizes research that could potentially enable super-capacitors to achieve energy densities of up to 0.180 kW-hr/kg (0.0818 kW-hr/lb_m). Ref. [20] provides some data collected from other publications on high performance conducting polymer-based super-capacitors that well surpass the capabilities of the current carbon-based super-capacitors. Being able to achieve these improvements in commercially available super-capacitors would substantially reduce system weight and could very well shift the scales in favor of the HPS configuration.

It is very common for electrified aircraft concepts to include EMs and batteries, which has prompted a great deal of research in advancing the state-of-the-art in these types of devices. However, impulsive ESDs, such as super-capacitors, do not receive the same spotlight. Such devices could provide benefits and even play key roles in enabling electrified aircraft concepts. The ability to provide and absorb impulsive power could help to minimize the presence of batteries and reduce the overall system weight. It could help address the transition of aircraft modes of operation, particularly when considering vertical-lift vehicles. Of course, there is the obvious application to the TEEM concept as well. With potential uses in aircraft propulsion systems, a case can be made to advance the state-of-the-art in super-capacitors. Improving metrics such as energy density, energy capacity, peak current, and capacitance would promote the practicality of the TEEM concept and may go on to otherwise improve electrified aircraft concepts.

Application of the TEEM concept to a standalone gas turbine engine will add weight via EMs, ESDs, and other supporting equipment. Additional torque supplied by the EMs may require the design of the shafts to be reconsidered, potentially requiring a sturdier and heavier design to withstand additional shear stresses. Furthermore, impacts on shaft inertias could impact the electric system requirements. While these are fair considerations, the impact is expected to be small given that the maximum torques supplied by the electric machines are less than ~3% of the maximum torque applied to the turbines through the combustion of fuel. While TEEM will add weight to the propulsion system in some areas, it could reduce weight in other areas. For instance, if the HPS EM is capable of accelerating the HPS to a speed that is sufficient to draw in enough air into the engine to support combustion, then the HPS EM could double as a starter motor. This could allow for the elimination of the APU, which adds weight on the order of 300 to 400 lb_m to the aircraft. Without an APU, there is no need for electric energy storage to support its starting. Thus those energy storage devices could potentially be eliminated or used for implementing the TEEM concept. If the power of the EM is not sufficient for starting the engine by itself, it could be used to assist the engine start, thereby prompting a reduction in the size of the APU and its supporting ESDs. Alternatively, the APU could be replaced by an additional EM that can be used with the HPS EM to supply shaft power to enable engine starting. At the very least, the additional EM should be lighter than the APU it replaces. Even if an APU is present, the ESDs used to support it and other aircraft systems could serve a dual purpose. Those ESDs could be replaced or supplemented by the ESDs used in the application of TEEM. The operability benefits achieved by TEEM also create opportunities for designing the engine in a way that improves fuel efficiency while also reducing the weight of the engine. Improvements in fuel efficiency could mean a reduction of onboard fuel storage which reduces overall weight. The reduced weight of the propulsion system and fuel could enable an increase in the passenger/cargo capacity or an extension of an aircraft's range. Further analysis is required to investigate the net benefit of implementing TEEM on the AGTF30 propulsion system, but the results to date seem to indicate that it has potential for enhancing the overall performance of electrified gas turbine propulsions systems and the aircrafts they propel.

VI. Conclusions

An electrical system architecture was defined for evaluating the feasibility and practicality of the Turbine Electrified Energy Management (TEEM) concept as implemented on a standalone turbofan. The electrical system has been modeled and integrated with an existing engine model that is representative of an advanced geared turbofan capable of producing 30,000lb_f of thrust at sea-level static conditions. The engine model incorporated health parameters to simulate the impact of engine component degradation in order to assure the electrical system is capable of providing consistent and substantial operability benefits throughout the engine's lifespan. Multiple configurations for implementing TEEM were considered, including the use of electric machines (EMs) on both spools and use of a single EM on the high pressure spool (HPS). Regarding the use of EMs on both spools, two variants were considered that implemented different strategies for dealing with excess power during deceleration transients. One of those variants reduced the power requirement on the low pressure spool (LPS) EM by roughly 33%. While the configuration with a single EM on the HPS eliminates the LPS EM, it may also require more energy storage. The total amount of useful energy capacity recommended is 0.8 to 3 kW-hr, depending on the configuration and how the worst-case transient scenario is defined. The recommended peak power of the HPS EM was 750 hp. The recommended peak power of the LPS EM was 610 and 410 hp, depending on the variant of the dual-spool configuration. The EMs are required to achieve their maximum torque within 0.8 and 3.7 s for the HPS and LPS EM respectively. This is well within the capabilities of the current state-of-the-art. Elimination or dual-use of engine and aircraft equipment that is used to apply the TEEM concept will help to offset penalties for implementing TEEM. While further investigation is required to validate the practicality of implementing TEEM in this application, including the quantification of benefits, the results appear to be within the realm of possibility. It was conjectured that the net benefits of the TEEM concept could be further enhanced through advances in impulsive energy storage devices such as super-capacitors.

Acknowledgments

The authors would like to acknowledge the Transformational Tools & Technologies (TTT) project under the Aeronautics Research Mission Directorate (ARMD) that has supported this work. The authors would also like to acknowledge those within NASA who contributed to the creation of the AGTF30 model that was utilized in this study including Jeffryes Chapman and Scott Jones. Gratitude is also extended to Mark Bell of Vantage Partners LLC who provided consulting with regards to electrical system modeling.

References

[1] Friedrich, C., and Robertson, P.A., "Hybrid-Electric Propulsion for Aircraft," Journal of Aircraft, Vol. 52, No. 1 (2015), pp. 176-189.

[2] Jansen, J.H., Bowman, C., Jankovsky, A., Dyson, R.., and Felder, J., "Overview of NASA Electrified Aircraft Propulsion Research for Large Subsonic Transports," AIAA Propulsion & Energy Forum, Atlanta, GA. 2017.

[3] Hyun, D., Perry, A.T., and Ansell, P.J., "A Review of Distributed Electric Propulsion Concepts for Air Vehicle Technology," AIAA Propulsion and Energy Forum, Cincinnati, OH. 2018.

[4] Johnson, W., Silva, C., and Solis, E., "Concept Vehicles for VTOL Air Taxi Operations," Report Number ARC-E-DAA-TN50731. 2018.

[5] Antcliff, K.R., and Capristan, F.M., "Conceptual Design of the Parallel Electric-Gas Architecture with Synergistic Utilization Scheme (PEGASUS) Concept," 18th AIAA/ISSMO Multidisciplinary Analysis and Optimization Conference, AIAA AVIATION Forum, Denver, CO. 2017.

[6] Culley, D., Kratz, J., and Thomas, G., "Turbine Electrified Energy Management (TEEM) For Enabling More Efficient Engine Designs," AIAA Propulsion & Energy Forum, Cincinnati, OH. 2018.

[7] Antcliff, K.R., Guynn, M.D., Marien, T.V., Wells, D.P.., Schneider, S.J., and Tong, M.T., "Mission Analysis and Aircraft Sizing of Hybrid-Electric Regional Aircraft," AIAA 2016-1028, AIAA SciTech, 54th AIAA Aerospace Sciences Meeting, San Diego, CA, January 4-8, 2016.

[8] Thomas, G., Culley, D., Kratz, J., and Fisher, K., "Dynamic Analysis of the hFan, a Parallel Hybrid Electric Turbofan Engine," AIAA Propulsion & Energy Forum, Cincinnati, OH, 2018.

[9] Kratz, J., Culley, D., Thomas, G., "A Control Strategy for Turbine Electrified Energy Management," AIAA Propulsion & Energy Forum, Indianapolis, IN. 2019.

[10] Chapman, J., and Litt, J., "Control Design for and Advanced Geared Turbofan Engine," AIAA Propulsion & Energy Forum, Atlanta, GA, 2017.

[11] Chapman, J., Lavelle, T., May, R., Litt, J., and Guo, T.-H., "Toolbox for the Modeling and Analysis of Thermodynamic Systems (T-MATS) User's Guide," NASA TM-2014-216638, 2014.

[12] Jones, S., Haller, W., and Tong, M., "An N+3 Technology Level Reference Propulsion System," NASA TM-2017-219501, 2017.
[13] Claus, R.W., Evans, A.L., Lylte, J.K. and Nichols, L.D., "Numerical Propulsion System Simulation," Computing Systems in Engineering, Vol 2, No. 4, pp 357-364, 1991.
[14] May, R.D., Csank, J., Lavelle, T.M., Litt, J. S., and Guo, T.-H., "A High-Fidelity Simulation of a Generic Commercial Aircraft Engine and Controller," Proceedings of the 46th AIAA/ASME/SAE/ASEE Joint Propulsion Conference, AIAA-2010- 6630, Nashville, TN, July 2010.
[15] Chapman, J., and Litt, J., "An Approach for Utilizing Power Flow Modeling for Simulations of Hybrid Electric Propulsion Systems," 2018 AIAA/IEEE Electric Aircraft Technologies Symposium, Cincinnati, OH, July 2018.
[16] Bradley, M.K., and Droney, C.K., "Subsonic Ultra Green Aircraft Research: Phase II -Volume II – Hybrid Electric Design Exploration," NASA/CR-2015-218704/Volume II. April, 2015.
[17] "125V Heavy Transportation Module Datasheet", Maxwell Technologies. URL: https://www.maxwell.com/images/documents/125V_Module_datasheet.pdf [retrieved 15 March 2019]
[18] Sadey, D., Csank, J., Hanlon, P., and Jansen, R., "A Generalized Power System Architecture Sizing and Analysis Framework," AIAA Propulsion & Energy Forum, Cincinnati, OH. 2018.
[19] "Alternative to traditional batteries moves a step closer to reality after exciting progress in super-capacitor technology" PHYS.ORG. February, 2018. URL: https://phys.org/news/2018-02-alternative-traditional-batteries-closer-reality.html [retrieved 24 May 2019]
[20] Shown, I., Ganguly, A., Chen, L.C., and Chen, K.-H., "Conducting polymer-based flexible supercapacitor," *Energy Science & Engineering*, Society of Chemical Industry and John Wiley & Sons Ltd. 2014. URL: https://onlinelibrary.wiley.com/doi/abs/10.1002/ese3.50 [retrieved 24 May 2019]